




Microstructure, morphology, and dielectric properties of in situ synthesized CCTO/CTO/TiO₂ composite ceramics

Yong Guo¹ , Junlang Tan¹, and Jingchang Zhao^{1,2,*}

¹School of Materials and Energy, Yunnan University, Kunming 650091, People's Republic of China

²Present address: School of Materials and Energy, Yunnan University, Kunming 650091, People's Republic of China

Received: 12 July 2021

Accepted: 4 November 2021

Published online:
27 January 2022

© The Author(s), under exclusive licence to Springer Science+Business Media, LLC, part of Springer Nature 2021

ABSTRACT

CaCu₃Ti₄O₁₂/CaTiO₃/TiO₂ (CCTO/CTO/TiO₂) composite ceramics were fabricated by an in situ route and sintered at 1040 °C for 8 h. The micrographs of FESEM show that the ceramics are dense and delicate, with an average particle size of about 0.9–1.4 μm. XPS found the existence of Cu⁺ and Ti³⁺, which was caused by the charge compensation reaction derived from part of Ti⁴⁺ ions entering the V^{''}_{Cu} to form the donor Ti^{''}_{Cu}. The impedance analysis shows that excessive CTO and TiO₂ significantly reduce the grain boundary resistance of CCTO/CTO/TiO₂ ceramics. Furthermore, it can be found that due to excessive CTO, TiO₂ reacts with segregated CuO to form CCTO again and reduce the CuO concentration at the grain boundaries. Therefore, this significantly reduces the grain boundary width, resulting in a colossal dielectric constant of 9.0×10^5 at 30 Hz.

1 Introduction

The development of capacitors with a giant dielectric constant is of great significance given devices' functionalization, miniaturization, and the actual industrial application requirement [1–7]. The perovskite-like materials Copper Calcium Titanate (CaCu₃Ti₄O₁₂, CCTO) with body-centered cubic Im $\bar{3}$ structure has been widely investigated owing to their permittivity (ϵ') in the order of 10^3 – 10^5 with excellent temperature stability over a wide temperature range from 100 to 500 °C [8–16]. Because of their giant

permittivity, CCTO materials have potential micro-electronics applications such as intelligent distributed grid systems, distributed energy storage systems, Super-capacitor, and memory (DRAM) devices [17–22]. However, the high low-frequency dielectric loss ($\tan \delta$) hinders its many commercial applications [6, 21, 23]. Thus, investigating the cause of high $\tan \delta$ value and giant dielectric constant value is a substantial issue that should be intensively performed for its practical application in the industrial field [2, 22–25].

For the moment, the huge dielectric mechanism of CCTO is interpreted as possibly related to various

Address correspondence to E-mail: jchzhao@ynu.edu.cn

barrier models such as surface barrier layers, domains, and grain boundaries [26–31]. Sinclair et al. have proposed in 2002 that the internal layer barrier capacitance (IBLC) is related to the semiconducting grain and insulating grain boundary [30]. Zhang et al. have reported in 2006 that the surface-layer effect could well explain these phenomena [29]. Paulo R Bueno et al. have put forward in 2011 that the polaronic stacking fault defect model explains the giant dielectric response materials [27]. Although most researchers have accepted the IBLC mechanism to interpret of electrical properties of perovskite polycrystalline material, it can not reasonably explain the dielectric mechanism of the single crystal [32]. At the same time, many researchers have well adjusted the dielectric properties through metal ion doping, blending, structural adjustment, and other methods, such as Sr^{2+} [11], Nd^{3+} [33], Mg^{2+} [34], Zn^{2+} [35], Zr^{4+} [36], and other single element doping, Al_2O_3 [37], PVDF [38], TiO_2 [39], and other oxides are compounded as the second phase. Herein, it is an urgent issue to understand the dielectric nature of CCTO by modulating the dielectric constant and microstructure evolution [1–3, 23].

To further enhance the dielectric properties of CCTO ceramics and study its mechanism, the perovskite material calcium titanate (CaTiO_3 , CTO) with a similar structure and low resistance, and TiO_2 with stable dielectric properties are compounded into CCTO. It is anticipated that the composite of CTO and TiO_2 into CCTO may affect the electrical dielectric behaviors. As known, Copper Calcium Titanate, calcium titanate, and titanium dioxide ($\text{CaCu}_3\text{Ti}_4\text{O}_{12}/\text{CaTiO}_3/\text{TiO}_2$, CCTO/CTO/ TiO_2) composite using in situ routes were rarely reported. Moreover, the dielectric properties of CCTO/CTO/ TiO_2 composites ceramics have been hardly discussed. Therefore, it is of great significance to investigate the effect of the composite of CTO and TiO_2 into CCTO on the dielectric nature and microstructure evolution of CCTO ceramics for exploring the colossal dielectric materials in the application of electronic devices.

In this work, the traditional solid-state method was used to fabricate the $\text{Ca}_{1+x}\text{Cu}_3\text{Ti}_{4.1+x}\text{O}_{12}$ ($x = 0.1, 0.2, 0.3$) ceramics. The microstructure, dielectric properties, valence states, and impedance of the materials were analyzed systematically.

2 Experiments

2.1 Synthesis processes

In this experiment, different ratios of CCTO/CTO/ TiO_2 composite powders are prepared by in situ synthesis, and the corresponding pure CCTO and CCTO/CTO/ TiO_2 composite ceramics ($\text{Ca}_{1+x}\text{Cu}_3\text{Ti}_{4.1+x}\text{O}_{12}$, $x = 0.1, 0.2, 0.3$) were prepared by the traditional solid-state reaction method. Initially, the mixture of CaCO_3 (99.99%, purity), CuO (99%, purity), and TiO_2 (99%, purity) was milled in ethanol for 24 h with ZrO_2 balls, and then the dried mixtures were calcined in air for 8 h at 930 °C. The calcined powder was ground again. Polyvinyl alcohol (PVA, 5%) was used as a binder and hydraulically pressed into green pellets with a diameter of 12 mm and a thickness of 2 mm. After slow heating (150 °C/h) up to 550 °C to remove PVA, the pellets were sintered in air at 1040 °C for 8 h followed by furnace cooling. Meanwhile, the composite ceramic samples with different proportions are referred to as Sample-1, Sample-2, Sample-3, and Sample-4, respectively.

2.2 Structure characterization

XRD apparatus (Rigaku D/Max 2500 PC, Japan) was executed to determine the crystal phase composition of the samples. The field emission scanning electron microscope (FESEM, Nano SEM 450, Germany) with a backscattered electrons detector and X-ray energy dispersive spectrometer (EDS) were examined the microstructures and elemental composition of pellets sputtered-coated with an Au film. The X-Ray photoelectron spectroscopy (XPS, Thermo Fisher K-Alpha +, USA) study was carried on a photoelectron spectrometer equipped with an Al $K\alpha$ radiation source (1486.6 eV) to the valence states of elements.

2.3 Measurement of electrical property

In order to measure the electrical properties of the ceramics, the polished sintered ceramics were plated with silver for 6 min on the 12 Ma ETD3000 sputtering silver plating device. The resistance and impedance characteristics of all ceramic samples are measured by an Agilent 4284 A precision impedance analyzer in the frequency range of 20 Hz–1 MHz at room temperature.

3 Result and discussion

3.1 Phase analyses

The XRD spectra of all powders are shown in Fig. 1, and two-phase structures of CaTiO_3 and CCTO can be found. The XRD patterns of all ceramic samples are presented in Fig. 2. It can be found that the standard pattern of CCTO ceramics (PDF#75-2188) with cubic perovskite structure and space group $\text{Im}\bar{3}$ can be well-matched with the diffraction peak sintered ceramics. This lattice parameter is calculated, and its change trend is in line with our experimental design, as shown in Table 1. A small amount of CaTiO_3 (PDF#81-0561) and TiO_2 (PDF#21-1276) is found in the CCTO/CTO/ TiO_2 ceramics, but the second phase TiO_2 and CaTiO_3 were not founded in the pure CCTO ceramics. These results show that pure CCTO ceramics and a ternary structure ceramic composed of CCTO, CTO, and TiO_2 were successfully synthesized.

3.2 Morphology structures

The FESEM micrograph of the ceramic specimens with the polished and high-temperature etched surface is displayed in Fig. 3. The mean sizes of these ceramics were measured by the software Image-Pro Plus 6.0 and summarized in Table 1. At the same time, the grain size distribution range is shown in Fig. 4. The micrograph of pure CCTO shows larger grains with a mean grain size of about $27\ \mu\text{m}$, as presented in Fig. 3a. Such grains of similar size have also been reported in the literature [34, 37, 40].

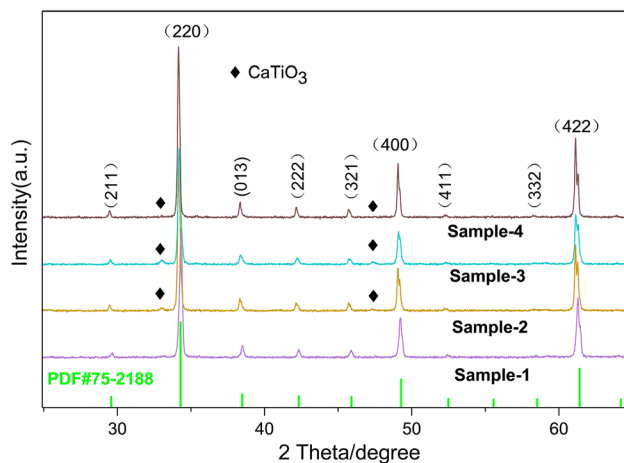


Fig. 1 XRD spectra of all powders

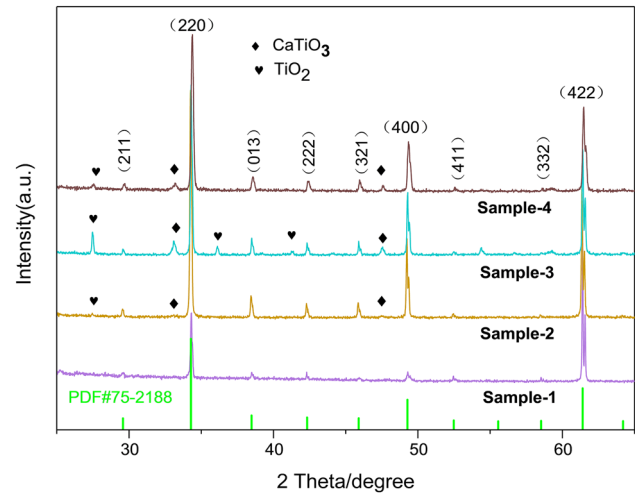


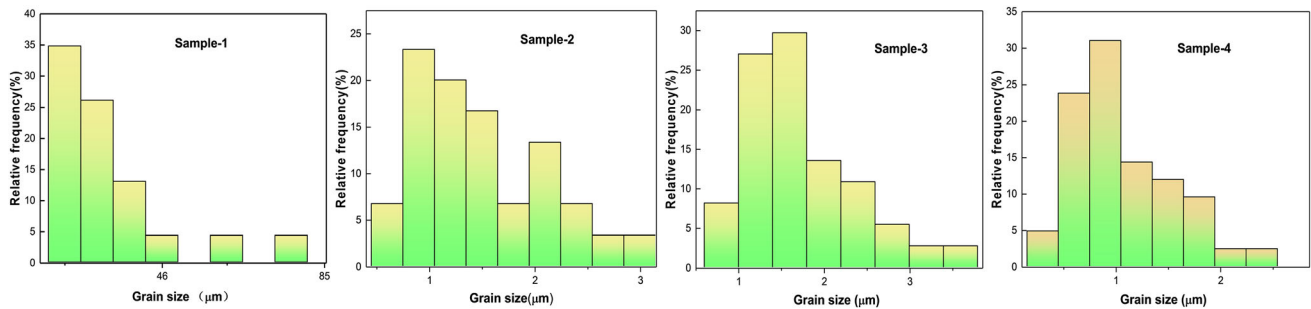
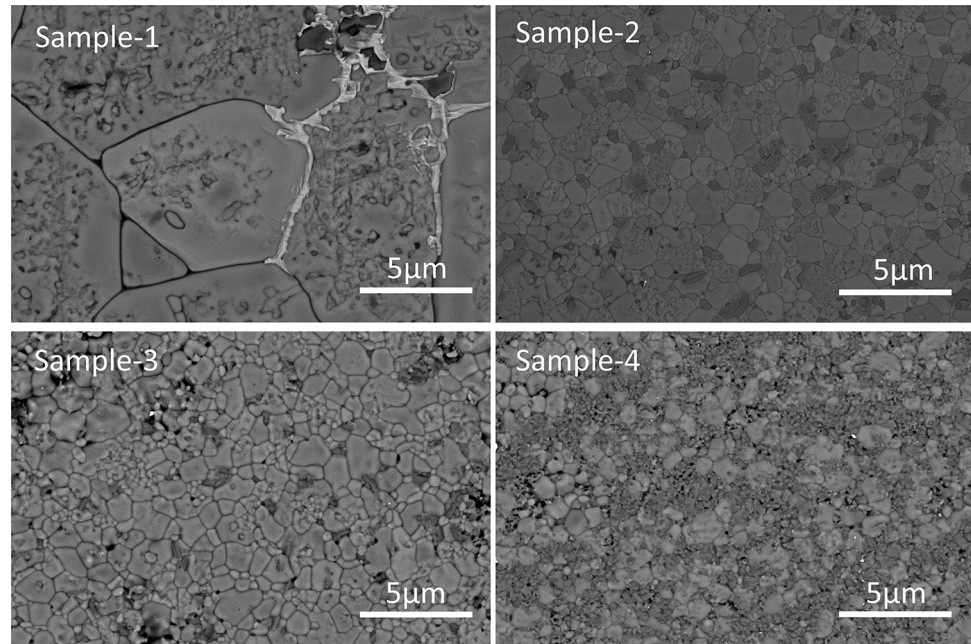
Fig. 2 XRD spectra of all ceramic samples

Besides, there is an apparent segregation phenomenon in the grain boundaries of pure CCTO, which is estimated to be liquid CuO infiltrated under high-temperature sintering. CuO is segregated in the grain boundary, reported in other literature [7, 41]. It can be seen that the addition of CTO and TiO_2 into the CCTO system has a pronounced effect on the microstructure of CCTO ceramics. Discontinuous grain growth occurred in CCTO/CTO/ TiO_2 composite ceramics, the porosity of all samples is reduced, large grains were scattered around small grains, and no segregation occurs at grain boundaries, as display in Fig. 3b–d, and Fig. 4. The absence of segregation CuO in the CCTO/CTO/ TiO_2 composite ceramics may be due to the resynthesis of CCTO by the presence of the second phase CTO and TiO_2 .

Interestingly, the grain size of samples decreases with the increase of CaTiO_3 content. This may be that part of CaTiO_3 and TiO_2 exists in the grain boundaries of CCTO, limiting the growth of CCTO grains. Consequently, it is suggested that the addition of CTO and TiO_2 into the CCTO system could improve the grain size and the densification of CCTO. Besides, Fig. 5 shows the EDS results of Sample-3, where it can be seen that the sample has a Ca, Ti, Cu, O component. In addition, the energy spectrum analysis results of the remaining samples are shown in Fig. S1, and the corresponding atomic percentages are shown in Table S1. The content changes of Ca, Ti, Cu, and O are consistent with the experimental design.

Table 1 Grain size, lattice parameters, dielectric constant, and loss of all ceramics sample

Sample label	Mean/ μm	Lattice parameters	DC (30 Hz)	DL (30 Hz)	DC (100 Hz)	DL (100 Hz)	DC (1 kHz)	DL (1 kHz)
Sample-1	27.0	7.3902	53,000	0.92	47,000	0.36	42,000	0.11
Sample-2	1.4	7.391	980,000	1.56	440,000	1.62	69,000	2.34
Sample-3	1.3	7.394	770,000	1.35	402,000	1.22	120,000	1.24
Sample-4	0.9	7.398	330,000	1.16	88,000	1.17	27,000	1.15

Fig. 3 FESEM micrograph of Sample-1 (a), Sample-2 (b), Sample-3 (c), and Sample-4 (d)**Fig. 4** The grain size distribution diagrams of Sample-1, Sample-2, Sample-3, and Sample-4

3.3 Dielectric properties

The frequency dependence of the permittivity ϵ_r for specimens is presented in Fig. 3a. All samples showed high permittivity ϵ_r (above 10^4) in the frequency range of 20 Hz–1 MHz. In Fig. 3a, a phenomenon can be observed. Compared with pure CCTO ceramics, the ϵ_r of CCTO/CTO/TiO₂ composite ceramics is more prominent. In the range of

20–500 Hz, the ϵ_r of CCTO/CTO/TiO₂ composite ceramics is much larger than pure CCTO and is at the giant dielectric level. Also, in the range of 500 Hz–10 kHz, the ϵ_r of the CCTO/CTO/TiO₂ composite ceramics is significantly greater than that of pure CCTO ceramics. The most significant ϵ_r appears in Sample-2, especially in the frequency range of 20 to 500 Hz, the ϵ_r were more outstanding than other samples. At 100 Hz, the dielectric constants of all

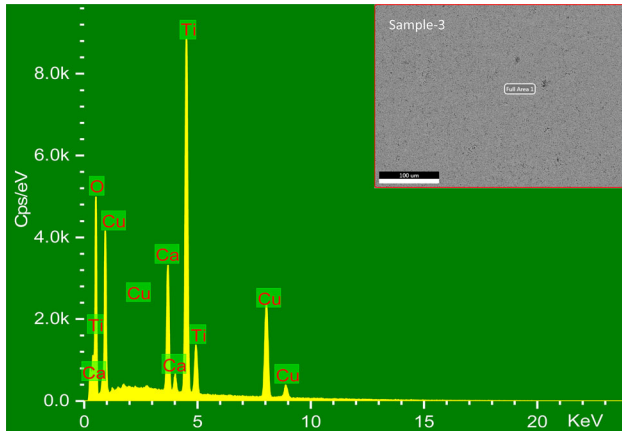
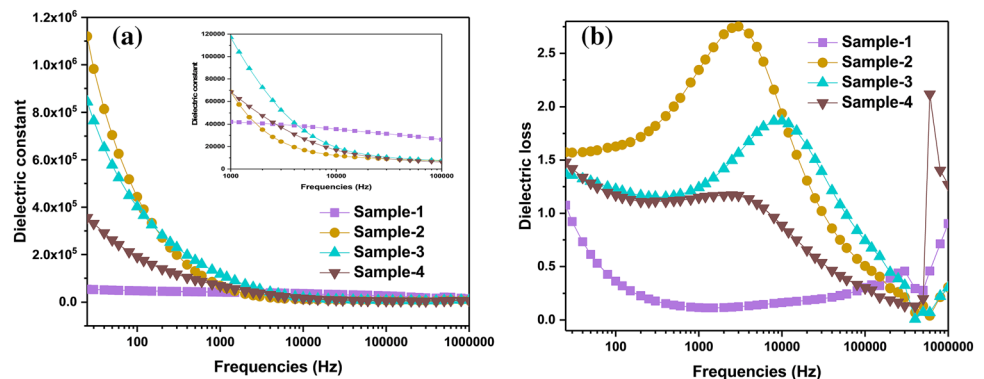


Fig. 5 EDS spectrum of Sample-3

samples are approximately 47,000 (Sample-1), 440,000 (Sample-2), 402,000 (Sample-3), and 88,000 (Sample-4), respectively. These samples all show a similar dielectric response trend ϵ_r decreases suddenly and sharply with the increases in frequency, and it does not reach stability until 10 kHz, which offers a typical Debye-type dipole relaxation [42, 43]

The frequency dependence of dielectric loss $\tan \delta$ for all ceramics is display in Fig. 3b. It can be intuitively observed from Fig. 6b that in the intermediate and low-frequency range, the $\tan \delta$ value of CCTO/CTO/TiO₂ composite ceramics is more excellent than for Sample-1, limiting their practicality application. Interestingly, in the high-frequency range, the $\tan \delta$ value of CCTO/CTO/TiO₂ composite ceramics is significantly reduced and is lower than pure CCTO ceramic samples. This result illuminates that CCTO/CTO/TiO₂ composite ceramics can be applied in the high-frequency range.

Fig. 6 Frequency dependence of dielectric responses for Sample-1, Sample-2, Sample-3, and Sample-4, (a) dielectric constant ϵ_r , (b) dielectric loss $\tan \delta$



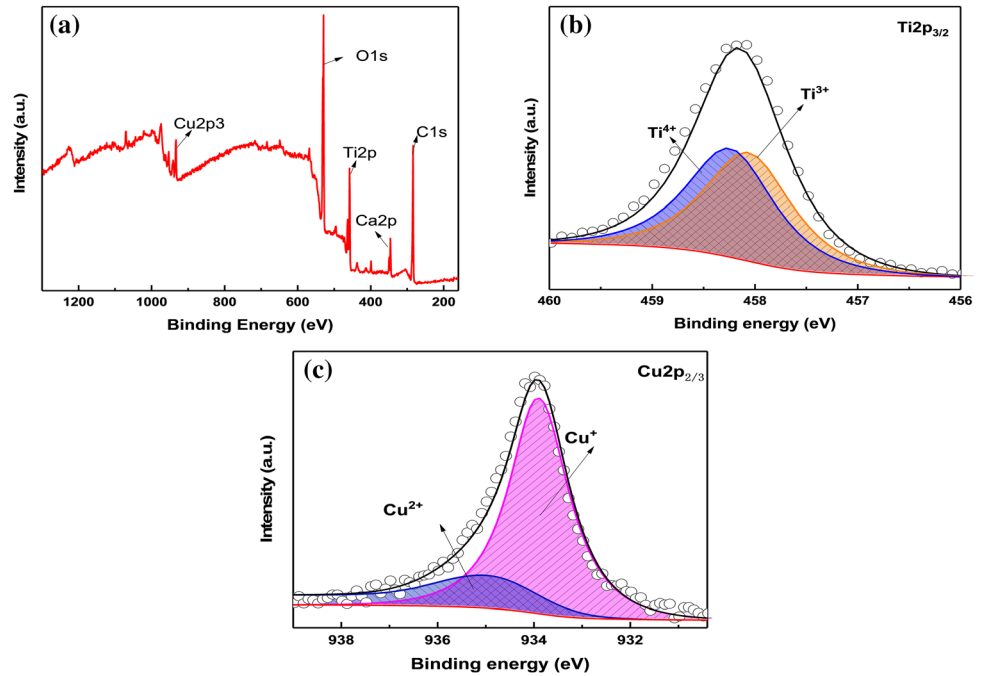
3.4 XPS analyses

X-Ray photoemission spectroscopy (XPS) was used to study the surface chemical states of Ti and Cu in Sample-3. Figure 7a shows the XPS spectrum, which contains the elemental peaks of O, Ca, Cu, and Ti. To further study the chemical state of these elements, fine spectrum scanning was used the study as demonstrated in Fig. 7b, c, respectively. As can be found in Fig. 7c, the two components make up the peak of Cu 2p_{3/2}. The element with the lowest binding energy state is associated with Cu⁺ in 933.98 eV, and the peaks with the highest binding energy state are attributed to Cu²⁺ in 935.02 eV. The fitted Ti 2p_{3/2} spectra are presented in Fig. 7b, which shows the main component of the sample at 459.3 eV, which is related to the Ti⁴⁺, and the small sub-peak at 458.4 eV corresponds to that of Ti³⁺. Therefore, it can be concluded that Cu⁺ and Ti³⁺ ions coexist in the CCTO/CTO/TiO₂ composites. Zhao et al. reported in 2012 that the existence of Cu⁺ and Ti³⁺ is due to the formation of negatively charged defects V_{Cu}^{''} after Cu²⁺ ions leaving the lattice, which makes Ti⁴⁺ enter and occupies the position of Cu²⁺ to cause donor defects Ti_{Cu}^{••}. Furthermore, the remaining positive charge is compensated by the chemical reaction between Cu²⁺ and Ti⁴⁺. This phenomenon is consistent with our experimental results. The existence of Cu⁺ and Ti³⁺ in the grains promotes the formation of semiconductor grains and the appearance of a high dielectric constant in CCTO ceramic [7].

3.5 Impedance spectrum analysis

The Cole–Cole plots and equivalent circuits are shown in Fig. 8, which can illustrate the electrical behavior of ceramics at room temperature. There are two dielectric relaxations in all of the ceramics by the

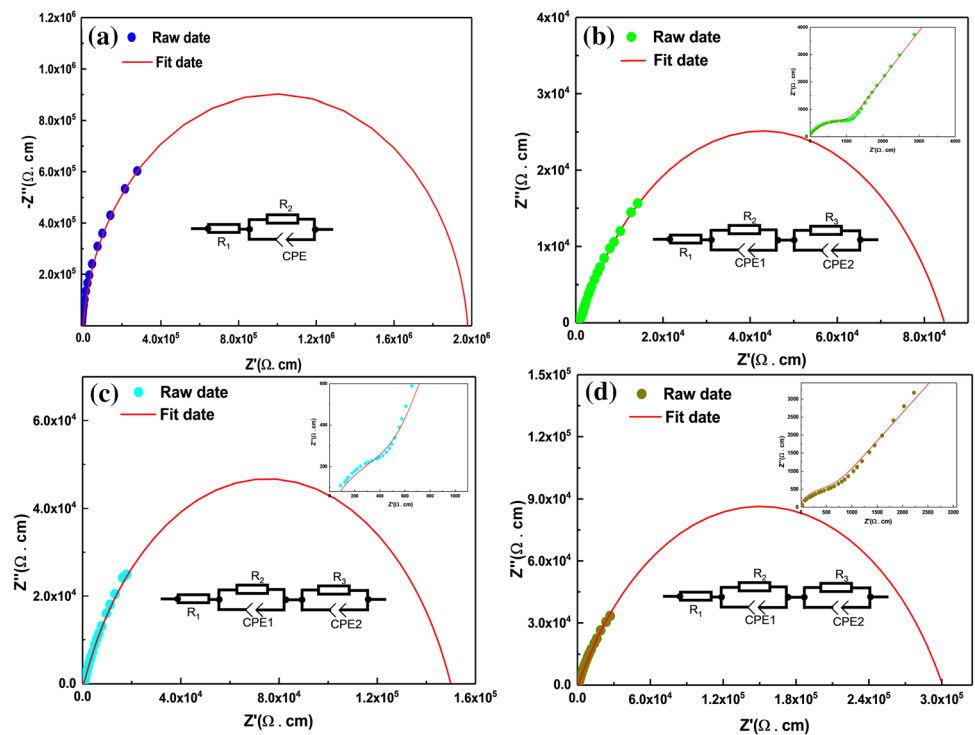
Fig. 7 X-Ray photoemission spectroscopy (XPS) spectra, (a) survey spectrum, (b) Ti 2p_{3/2}, (c) Cu 2p_{3/2} of Sample-3



plots. According to the IBLC model, the diameter of the arc and the intercept of the X-axis usually correspond to different response mechanisms. The equivalent circuit diagram of the corresponding sample is drawn for further understanding. The grain resistance, nanocrystalline resistance, and grain boundary

resistance are represented in the circuit by R_g , R_{nano} , and R_{gb} . While CPE describes the constant phase angle element, and the circuits are illustrated in Fig. 8. The corresponding equivalent electric circuit model was used to fit the dielectric response of all ceramic samples. The detailed electrical parameters

Fig. 8 The Cole–Cole plot of impedance and the equivalent circuit for Sample-1 (a), Sample-2 (b), Sample-3 (c), and Sample-4 (d), respectively



are shown in Table 2. It was found that the fitted data are consistent with the measured data, as shown in Fig. 8, which shows that the selected analog circuit is reasonable. By fitting the arc data, it is found that the R_{gb} of CCTO/CTO/TiO₂ composite is significantly lower than that of pure CCTO ceramics. The decrease in the CCTO/CTO/TiO₂ composite resistance may be that the excessive CTO and TiO₂ react with the segregated CuO again to form CCTO particles. Combined with the Fig. 3 FESEM micrograph, the pure CCTO has CuO segregated at the grain boundary.

In contrast, CCTO/CTO/TiO₂ composite ceramic does not segregate, and the existence of the CuO phase can indeed increase the resistance. Besides, with the increase of CTO content, the tiny grains around CCTO gradually increase, verifying the synthesis of CCTO by the reaction. The experimental results confirm the decrease of CuO at the grain boundary.

3.6 Discussion

The colossal dielectric behavior of the composite ceramics can be explained by the mechanism diagram shown in Fig. 9. The relationship between the effective constant (ϵ'_{eff}) of IBLC and the average grain size (d_{gr}), the width (d_{gb}) of grain boundary depletion layer, and the permittivity (ϵ_{gb}) in the grain boundary layer can be described by a simple brick wall model as:

$$\epsilon'_{eff} = \epsilon_{gb} \frac{d_{gr}}{d_{gb}} \tag{1}$$

It can be found that the thickness of the grain and grain boundary is of great significance to the permittivity of the CCTO system. For CCTO/CTO/TiO₂ composite ceramics, due to excess CTO and TiO₂ reacting with grain boundary segregation CuO to form CCTO, the grain boundary width is significantly reduced, increasing the dielectric constant of the system, as shown in Fig. 9d. These XPS results confirm the existence of Cu⁺ and Ti³⁺ due to the

charge compensation reaction. In Fig. 9c, the Cu²⁺ leaving the lattice to form CuO and segregation in the grain boundary at high temperature, after the acceptor defects V''_{Cu} with negatively charged left in the lattice is occupied by donor defects Ti'_{Cu} to form complex defects $Ti'_{Cu}V''_{Cu}$, which may enhance the effect of Ti ions replacing Cu positions and increase the grain semiconduction of CCTO/CTO/TiO₂ composite ceramic.

4 Conclusion

The ternary composite structure of Ca_{1+x}Cu₃Ti_{4.1+x}O₁₂ ceramic with $x = 0.1, 0.2, 0.3$, and pure CaCu₃Ti₄O₁₂ was constructed in situ synthesis method, and its ceramics were prepared by the traditional solid-phase reaction method. The excess TiO₂ is mainly used to compensate for the loss of Cu²⁺ during the high-temperature sintering of CCTO so that the crystal grains can achieve semiconductivity. The excess CTO and TiO₂ react with the high-temperature segregation CuO again to synthesize CCTO, which reduces the concentration of CuO at the grain boundary, thereby the width of the grain boundary. The XRD and EDS analysis confirmed that CCTO, CTO, and TiO₂ without impurity phases could be obtained. The FESEM results show that the growth of grains is restricted with the increase of CTO content, the grains are refined and dense, the grain boundary segregation is reduced, and the grain boundary becomes thinner. The XPS confirmed the existence of Cu⁺ and Ti³⁺ states in CCTO/CTO/TiO₂ composites ceramics.

Meanwhile, Impedance analysis using the IBLC model indicates the grain boundary resistance decreases drastically with the addition of CaTiO₃, which may originate from the reduction of the CuO in the grain boundary region. Compared with pure CCTO, the dielectric constant of the CCTO/CTO/TiO₂ composites ceramics has been dramatically improved to 9.0×10^5 in the low-frequency region, as shown in Table 1. In summary, such a colossal

Table 2 Electrical parameters of the equivalent circuit

Material	R_g	R_{nano}	R_{gb}	CPE1-T	CPE1-P	CPE2-T	CPE2-T
Sample-1	10	569	1,970,000	1.10E-08	0.94138		
Sample-2	90	1100	84,510	9.49E-08	0.7505	1.23E-06	0.69
Sample-3	10	553	140,000	9.01E-07	0.585	6.98E-07	0.75
Sample-4	7.5	370	299,890	1.30E-08	0.791	8.00E-07	0.6657

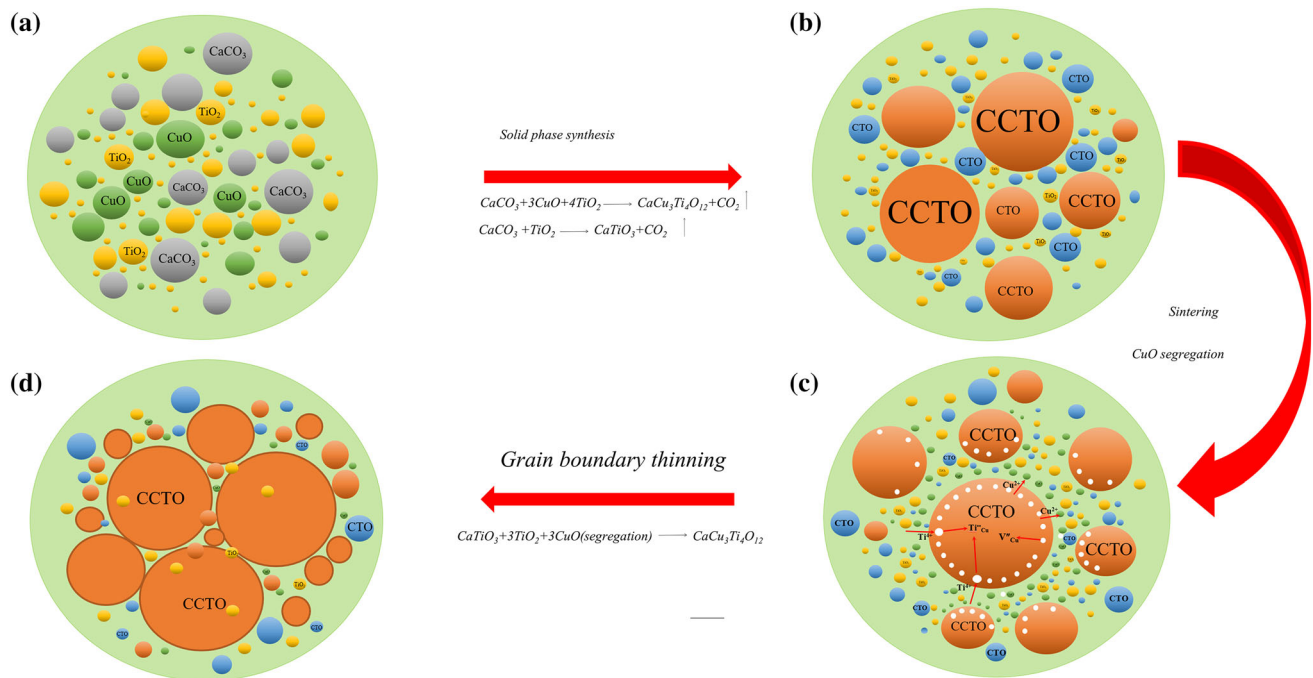


Fig. 9 The diagram of the huge dielectric formation mechanism of composite ceramics

dielectric constant is mainly due to the refinement and semiconductivity of grains and thinning grain boundary width.

Acknowledgements

This work was supported by the Natural Science Foundation of China (51562037) and Yunnan University Graduate Research and Innovation Fund (2020Z41). The authors thank Advanced Analysis and Measurement Center of Yunnan University for the sample testing service.

Declarations

Conflict of interest There are no conflict of interest to declare.

Supplementary Information: The online version contains supplementary material available at <http://doi.org/10.1007/s10854-021-07346-8>.

References

1. P. Mao, J. Wang, P. Xiao, L. Zhang, F. Kang, H. Gong, Colossal dielectric response and relaxation behavior in novel

system of Zr^{4+} and Nb^{5+} co-substituted $\text{CaCu}_3\text{Ti}_4\text{O}_{12}$ ceramics. *Ceram. Int.* **47**, 111–120 (2021)

2. J.A. Cortés, H. Moreno, S. Orrego, V.D.N. Bezzon, M.A. Ramírez, Dielectric and non-ohmic analysis of Sr^{2+} influences on $\text{CaCu}_3\text{Ti}_4\text{O}_{12}$ -based ceramic composites, *Materials Research Bulletin*, **134** (2021)
3. P. Mao, J. Wang, S. Liu, L. Zhang, Y. Zhao, L. He, Grain size effect on the dielectric and non-ohmic properties of $\text{CaCu}_3\text{Ti}_4\text{O}_{12}$ ceramics prepared by the sol-gel process. *J. Alloy. Compd.* **778**, 625–632 (2019)
4. J. Zhao, J. Liu, G. Ma, Preparation, characterization and dielectric properties of $\text{CaCu}_3\text{Ti}_4\text{O}_{12}$ ceramics. *Ceram. Int.* **38**, 1221–1225 (2012)
5. L.F. Xu, K. Sun, X. Feng, H.B. Xiao, R.L. Wang, C.P. Yang, Abnormal capacitance–voltage behaviors of bismuth-doped $\text{CaCu}_3\text{Ti}_4\text{O}_{12}$ ceramics. *Int. J. Modern Phys. B*, **31** (2017)
6. X.W. Wang, P.B. Jia, L.Y. Sun, B.H. Zhang, X.E. Wang, Y.C. Hu, J. Shang, Y.Y. Zhang, Improved dielectric properties in $\text{CaCu}_3\text{Ti}_4\text{O}_{12}$ ceramics modified by TiO_2 . *J. Mater. Sci.: Mater. Electron.* **29**, 2244–2250 (2017)
7. J. Zhao, H. Zhao, Z. Zhu, Influence of sintering conditions and CuO loss on dielectric properties of $\text{CaCu}_3\text{Ti}_4\text{O}_{12}$ ceramics. *Mater. Res. Bull.* **113**, 97–101 (2019)
8. J. Yang, M. Shen, L. Fang, The electrode/sample contact effects on the dielectric properties of the $\text{CaCu}_3\text{Ti}_4\text{O}_{12}$ ceramic. *Mater. Lett.* **59**, 3990–3993 (2005)

9. C.C. Calvert, W.M. Rainforth, D.C. Sinclair, A.R. West, EELS characterization of bulk $\text{CaCu}_3\text{Ti}_4\text{O}_{12}$ ceramics. *Micron* **37**, 412–419 (2006)
10. Z. Kafi, A. Kompany, H. Arabi, A. Khorsand Zak, The effect of cobalt-doping on microstructure and dielectric properties of $\text{CaCu}_3\text{Ti}_4\text{O}_{12}$ ceramics. *J. Alloys Compd.* **727**, 168–176 (2017)
11. S. Orrego, J.A. Cortés, R.A.C. Amoresi, A.Z. Simões, M.A. Ramírez, Photoluminescence behavior on Sr^{2+} modified $\text{CaCu}_3\text{Ti}_4\text{O}_{12}$ based ceramics. *Ceram. Int.* **44**, 10781–10789 (2018)
12. M.K. Pradhan, T.L. Rao, L. Karna, S. Dash, Giant dielectric response in (Sr, Sb) codoped $\text{CaCu}_3\text{Ti}_4\text{O}_{12}$ ceramics: a novel approach (2018)
13. A. Skwarek, R.P. Socha, D. Szwagierczak, P. Zachariasz, Investigation of the microstructure and chemical composition of $\text{CaCu}_3\text{Ti}_4\text{O}_{12}$ multilayer elements using SEM, EDS, and XPS. *Acta Phys. Pol., A* **134**, 318–321 (2018)
14. L. Zhao, R. Xu, Y. Wei, X. Han, C. Zhai, Z. Zhang, X. Qi, B. Cui, J.L. Jones, Giant dielectric phenomenon of $\text{Ba}_{0.5}\text{Sr}_{0.5}\text{TiO}_3/\text{CaCu}_3\text{Ti}_4\text{O}_{12}$ multilayers due to interfacial polarization for capacitor applications. *J. Eur. Ceramic Soc.* **39**, 1116–1121 (2019)
15. R. Djafar, K. Boumchedda, A. Chaouchi, D. Fasquelle, K. Sedda, S. Brahimi, K. Khalfaoui, M. Bououdina, CuO addition and sintering temperature dependence of structural, microstructural and dielectric properties of $\text{CaCu}_3\text{Ti}_4\text{O}_{12}$ ceramics. *Mater. Chem. Phys.* **256** (2020)
16. H. Moreno, J.A. Cortés, F.M. Praxedes, S.M. Freitas, M.V.S. Rezende, A.Z. Simões, V.C. Teixeira, M.A. Ramirez, Tunable photoluminescence of $\text{CaCu}_3\text{Ti}_4\text{O}_{12}$ based ceramics modified with tungsten. *J. Alloys Compd.* **850** (2021).
17. P. Fiorenza, R. Lo Nigro, A. Sciuto, P. Delugas, V. Raineri, R.G. Toro, M.R. Catalano, G. Malandrino, Perovskite $\text{CaCu}_3\text{Ti}_4\text{O}_{12}$ thin films for capacitive applications: From the growth to the nanoscopic imaging of the permittivity. *J. Appl. Phys.* **105** (2009).
18. C. Mu, H. Zhang, Y. Liu, Y. Song, P. Liu, Rare earth doped $\text{CaCu}_3\text{Ti}_4\text{O}_{12}$ electronic ceramics for high frequency applications. *J. Rare Earths* **28**, 43–47 (2010)
19. J.-W. Lee, J.-H. Koh, Grain size effects on the dielectric properties of $\text{CaCu}_3\text{Ti}_4\text{O}_{12}$ ceramics for supercapacitor applications. *Ceram. Int.* **41**, 10442–10447 (2015)
20. D.S. Saidina, A. Norshamira, M. Mariatti, Dielectric and thermal properties of CCTO/epoxy composites for embedded capacitor applications: mixing and fabrication methods. *J. Mater. Sci.: Mater. Electron.* **26**, 8118–8129 (2015)
21. S. Kaur, A. Kumar, A.L. Sharma, D.P. Singh, Dielectric and energy storage behavior of $\text{CaCu}_3\text{Ti}_4\text{O}_{12}$ nanoparticles for capacitor application. *Ceram. Int.* **45**, 7743–7747 (2019)
22. L. Zhang, F. Song, X. Lin, D. Wang, High-dielectric-permittivity silicone rubbers incorporated with polydopamine-modified ceramics and their potential application as dielectric elastomer generator. *Mater. Chem. Phys.* **241** (2020)
23. X. Yue, W. Long, J. Liu, S. Pandey, S. Zhong, L. Zhang, S. Du, D. Xu, Enhancement of dielectric and non-ohmic properties of graded Co doped $\text{CaCu}_3\text{Ti}_4\text{O}_{12}$ thin films. *J. Alloys Compd.* **816** (2020)
24. G. Wu, Z. Yu, K. Sun, R. Guo, X. Jiang, C. Wu, Z. Lan, Effect of $\text{CaCu}_3\text{Ti}_4\text{O}_{12}$ dopant on the magnetic and dielectric properties of high-frequency MnZn power ferrites. *J. Magnet. Magnet. Mater.* **513** (2020)
25. P. Mao, J. Wang, L. Zhang, Z. Wang, F. Kang, S. Liu, D.B.K. Lim, X. Wang, H. Gong, Significantly enhanced breakdown field with high grain boundary resistance and dielectric response in $_{0.1}\text{Na}_{0.5}\text{Bi}_{0.5}\text{TiO}_{3-0.9}\text{BaTiO}_3$ doped $\text{CaCu}_3\text{Ti}_4\text{O}_{12}$ ceramics. *J. Eur. Ceram. Soc.* **40**, 3011–3018 (2020)
26. M.M. Ahmad, Giant dielectric constant in $\text{CaCu}_3\text{Ti}_4\text{O}_{12}$ nanoceramics. *Appl. Phys. Lett.* **102** (2013)
27. W.C. Ribeiro, E. Joanni, R. Savu, P.R. Bueno, Nanoscale effects and polaronic relaxation in $\text{CaCu}_3\text{Ti}_4\text{O}_{12}$ compounds. *Solid State Commun.* **151**, 173–176 (2011)
28. P.R. Bueno, R. Tararan, R. Parra, E. Joanni, M.A. Ramírez, W.C. Ribeiro, E. Longo, J.A. Varela, A polaronic stacking fault defect model for $\text{CaCu}_3\text{Ti}_4\text{O}_{12}$ material: an approach for the origin of the huge dielectric constant and semiconducting coexistent features. *J. Phys. D Appl. Phys.* **42** (2009)
29. C.C. Wang, L.W. Zhang, Surface-layer effect in $\text{CaCu}_3\text{Ti}_4\text{O}_{12}$. *Appl. Phys. Lett.* **88** (2006)
30. D.C. Sinclair, T.B. Adams, F.D. Morrison, A.R. West, $\text{CaCu}_3\text{Ti}_4\text{O}_{12}$: one-step internal barrier layer capacitor. *Appl. Phys. Lett.* **80**, 2153–2155 (2002)
31. P. Lunkenheimer, R. Fichtl, S.G. Ebbinghaus, A. Loidl, Nonintrinsic origin of the colossal dielectric constants in $\text{CaCu}_3\text{Ti}_4\text{O}_{12}$. *Phys. Rev. B* **70** (2004)
32. H. Lin, W. Xu, H. Zhang, C. Chen, Y. Zhou, Z. Yi, Origin of high dielectric performance in fine grain-sized $\text{CaCu}_3\text{Ti}_4\text{O}_{12}$ materials. *J. Eur. Ceram. Soc.* **40**, 1957–1966 (2020)
33. Y. Wang, L. Ni, X.M. Chen, Effects of Nd-substitution on microstructures and dielectric characteristics of $\text{CaCu}_3\text{Ti}_4\text{O}_{12}$ ceramics. *J. Mater. Sci.: Mater. Electron.* **22**, 345–350 (2010)
34. L. Ni, X.M. Chen, Enhanced giant dielectric response in Mg-substituted $\text{CaCu}_3\text{Ti}_4\text{O}_{12}$ ceramics. *Solid State Commun.* **149**, 379–383 (2009)
35. D. Xu, K. He, R. Yu, X. Sun, Y. Yang, H. Xu, H. Yuan, J. Ma, High dielectric permittivity and low dielectric loss in sol-gel derived Zn doped $\text{CaCu}_3\text{Ti}_4\text{O}_{12}$ thin films. *Mater. Chem. Phys.* **153**, 229–235 (2015)

36. Y. Su, W. Zhang, Dielectric properties and electrical conductivity of $\text{CaCu}_3\text{Ti}_4\text{O}_{12}$ ceramics doped with Zr^{4+} . *J. Wuhan Univ. Technol-Mater. Sci. Ed.* **28**, 343–346 (2013)
37. M.F.A. Rahman, M.J. Abu, S.A. Karim, R.A. Zaman, M.F. Ain, Z.A. Ahmad, J.J. Mohamed, Microwave dielectric properties of $\text{CaCu}_3\text{Ti}_4\text{O}_{12}\text{-Al}_2\text{O}_3$ composite (2016)
38. B. Ghosh, R.M. Tamayo Calderón, R. Espinoza-González, S.A. Hevia, Enhanced dielectric properties of PVDF/ $\text{CaCu}_3\text{Ti}_4\text{O}_{12}$: Ag composite films. *Mater. Chem. Phys.* **196**, 302–309 (2017)
39. J. Wang, Y. Long, Y. Sun, X. Zhang, H. Yang, B. Lin, Fabrication and enhanced dielectric properties of polyimide matrix composites with core-shell structured $\text{CaCu}_3\text{Ti}_4\text{O}_{12}@/\text{TiO}_2$ nanofibers. *J. Mater. Sci.: Mater. Electron.* **29**, 7842–7850 (2018)
40. A. Rajabtabar-Darvishi, R. Bayati, O. Sheikhejad-Bishe, L.D. Wang, W.L. Li, J. Sheng, W.D. Fei, Giant dielectric response and low dielectric loss in Al_2O_3 grafted $\text{CaCu}_3\text{Ti}_4\text{O}_{12}$ ceramics. *J. Appl. Phys.* **117** (2015).
41. J. Li, R. Jia, L. Hou, L. Gao, K. Wu, S. Li, The dimensional effect of dielectric performance in $\text{CaCu}_3\text{Ti}_4\text{O}_{12}$ ceramics: Role of grain boundary. *J. Alloy. Compd.* **644**, 824–829 (2015)
42. P. Liu, Y. Lai, Y. Zeng, S. Wu, Z. Huang, J. Han, Influence of sintering conditions on microstructure and electrical properties of $\text{CaCu}_3\text{Ti}_4\text{O}_{12}$ (CCTO) ceramics. *J. Alloy. Compd.* **650**, 59–64 (2015)
43. M.J. Abu, J.J. Mohamed, M.F. Ain, Z.A. Ahmad, Phase structure, microstructure and broadband dielectric response of Cu nonstoichiometry $\text{CaCu}_3\text{Ti}_4\text{O}_{12}$ ceramic. *J. Alloy. Compd.* **683**, 579–589 (2016)

Publisher's Note Springer Nature remains neutral with regard to jurisdictional claims in published maps and institutional affiliations.